Period-one oscillation for photonic microwave transmission using an optically injected semiconductor laser

Sze-Chun Chan[1], **Sheng-Kwang Hwang**[1,2], **and Jia-Ming Liu**[1]

[1] *Department of Electrical Engineering, University of California, Los Angeles, Los Angeles, CA 90095-1594, USA*

[2] *Department of Electro-Optical Engineering, National Cheng Kung University, Tainan, 701, Taiwan, R.O.C.*

scchan@ucla.edu

Abstract: Optically injected semiconductor laser under period-one oscillation is investigated as a source for photonic microwave transmission over fiber. The period-one nonlinear dynamics of an optically injected laser is studied for the purpose of minimizing the microwave power penalty induced by chromatic dispersion. Over a large range of injection strengths and frequency detunings, we first obtain the mapping of the period-one oscillation characteristics, including the microwave frequency, the microwave power, and the single sideband (SSB) characteristics of the optical spectrum. By accounting for the fiber chromatic dispersion, we calculate its effect on the optical spectrum and the associated microwave power penalty. A mapping of the minimum microwave power deliverable after the maximum penalty is obtained. The system is shown to be least susceptible to the penalty when operated under strong injection with the frequency detuned above the Hopf bifurcation line. Microwave frequency beyond six times the relaxation resonance frequency can be effectively transmitted.

OCIS codes: (140.5960) semiconductor lasers; (140.3520) lasers, injection-locked; (350.4010) microwaves.

References and links

1. A. J. Seeds, "Microwave photonics," IEEE Trans. Microwave Theory Tech. **50**, 877–887 (2002).
2. N. Dagli, "Wide-bandwidth lasers and modulators for RF photonics," IEEE Trans. Microwave Theory Tech. **47**, 1151–1171 (1999).
3. A. Kaszubowska, P. Anandarajah, and L. P. Barry, "Multifunctional operation of a fiber Bragg grating in a WDM/SCM radio over fiber distribution system," IEEE Photon. Technol. Lett. **16**, 605–607 (2004).
4. C. Lim, A. Nirmalathas, D. Novak, R. Waterhouse, and G. Yoffe, "Millimeter-wave broad-band fiber-wireless system incorporating baseband data transmission over fiber and remote LO delivery," J. Lightwave Technol. **18**, 1355–1363 (2000).
5. D. Novak, G. H. Smith, A. J. Lowery, H. F. Liu, and R. B. Waterhouse, "Millimetre-wave fibre-wireless transmission systems with reduced effects of fibre chromatic dispersion," Opt. Quantum Electron. **30**, 1021–1031 (1998).

#83240 - $15.00 USD Received 21 May 2007; revised 21 Oct 2007; accepted 22 Oct 2007; published 26 Oct 2007

6. C. Lim, D. Novak, A. Nirmalathas, and G. H. Smith, "Dispersion-induced power penalties in millimeter-wave signal transmission using multisection DBR semiconductor laser," IEEE Trans. Microwave Theory Tech. **49**, 288–296 (2001).
7. G. H. Smith, D. Novak, and Z. Ahmed, "Overcoming chromatic-dispersion effects in fiber-wireless systems incorporating external modulators," IEEE Trans. Microwave Theory Tech. **45**, 1410–1415 (1997).
8. U. Gliese, "Multi-functional fibre-optic microwave links," Opt. Quantum Electron. **30**, 1005–1019 (1998).
9. L. A. Johansson and A. J. Seeds, "Generation and transmission of millimeter-wave data-modulated optical signals using an optical injection phase-lock loop," J. Lightwave Technol. **21**, 511–520 (2003).
10. M. Hyodo, K. S. Abedin, and N. Onodera, "Generation of millimeter-wave signals up to 70.5 GHz by heterodyning of two extended-cavity semiconductor lasers with an intracavity electro-optic crystal," Opt. Commun. **171**, 159–169 (1999).
11. J. Han, B. J. Seo, Y. Han, B. Jalali, and H. R. Fetterman, "Reduction of fiber chromatic dispersion effects in fiber-wireless and photonic time-stretching system using polymer modulators," J. Lightwave Technol. **21**, 1504–1509 (2003).
12. D. Wake, C. R. Lima, and P. A. Davies, "Transmission of 60-GHz signals over 100 km of optical fiber using a dual-mode semiconductor laser source," IEEE Photon. Technol. Lett. **8**, 578–580 (1996).
13. K. Sato, "Semiconductor light sources for 40-Gb/s transmission systems," J. Lightwave Technol. **20**, 2035–2043 (2002).
14. K. S. Lee and C. Shu, "Stable and widely tunable dual-wavelength continuous-wave operation of a semiconductor laser in a novel Fabry-Perot grating-lens external cavity," IEEE J. Quantum Electron. **33**, 1832–1838 (1997).
15. K. E. Razavi and P. A. Davies, "Semiconductor laser sources for the generation of millimetre-wave signals," IEE Proc. Optoelectron. **145**, 159–163 (1998).
16. H. S. Ryu, Y. K. Seo, and W. Y. Choi, "Dispersion-tolerant transmission of 155-Mb/s data at 17 GHz using a 2.5-Gb/s-grade DFB laser with wavelength-selective gain from an FP laser diode," IEEE Photon. Technol. Lett. **16**, 1942–1944 (2004).
17. S. C. Chan, S. K. Hwang, and J. M. Liu, "Radio-over-fiber AM-to-FM upconversion using an optically injected semiconductor laser," Opt. Lett. **31**, 2254–2256 (2006).
18. S. C. Chan, S. K. Hwang, and J. M. Liu, "Radio-over-fiber transmission from an optically injected semiconductor laser in period-one state," SPIE **6468**, 646811 (2007).
19. S. K. Hwang, J. M. Liu, and J. K. White, "Characteristics of period-one oscillations in semiconductor lasers subject to optical injection," IEEE J. Sel. Top. Quantum Electron. **10**, 974–981 (2004).
20. S. C. Chan and J. M. Liu, "Frequency modulation on single sideband using controlled dynamics of an optically injected semiconductor laser," IEEE J. Quantum Electron. **42**, 699–705 (2006).
21. T. B. Simpson and F. Doft, "Double-locked laser diode for microwave photonics applications," IEEE Photon. Technol. Lett. **11**, 1476–1478 (1999).
22. T. B. Simpson, "Phase-locked microwave-frequency modulations in optically-injected laser diodes," Opt. Commun. **170**, 93–98 (1999).
23. S. C. Chan and J. M. Liu, "Tunable narrow-linewidth photonic microwave generation using semiconductor laser dynamics," IEEE J. Sel. Top. Quantum Electron. **10**, 1025–1032 (2004).
24. A. Kaszubowska, L. P. Barry, and P. Anandarajah, "Effects of intermodulation distortion on the performance of a hybrid radio/fiber system employing a self-pulsating laser diode transmitter," IEEE Photon. Technol. Lett. **15**, 852–854 (2003).
25. A. Kaszubowska, L. P. Barry, and P. Anandarajah, "Multiple RF carrier distribution in a hybrid radio/fiber system employing a self-pulsating laser diode transmitter," IEEE Photon. Technol. Lett. **14**, 1599–1601 (2002).
26. L. Noël, D. Wake, D. G. Moodie, D. D. Marcenac, L. D. Westbrook, and D. Nesset, "Novel techniques for high-capacity 60-GHz fiber-radio transmission systems," IEEE Trans. Microwave Theory Tech. **45**, 1416–1423 (1997).
27. P. Sabouréau, J. P. Foing, and P. Schanne, "Injection-locked semiconductor lasers with delayed optoelectronic feedback," IEEE J. Quantum Electron. **33**, 1582–1591 (1997).
28. T. B. Simpson, J. M. Liu, K. F. Huang, and K. Tai, "Nonlinear dynamics induced by external optical injection in semiconductor lasers," Quantum Semiclass. Opt. **9**, 765–784 (1997).
29. T. B. Simpson, J. M. Liu, and A. Gavrielides, "Small-signal analysis of modulation characteristics in a semiconductor laser subject to strong optical injection," IEEE J. Quantum Electron. **32**, 1456–1468 (1996).
30. J. M. Liu, Photonic Devices. Cambridge (2005).

#83240 - $15.00 USD Received 21 May 2007; revised 21 Oct 2007; accepted 22 Oct 2007; published 26 Oct 2007

31. S. K. Hwang, J. M. Liu, and J. K. White, "35-GHz intrinsic bandwidth for direct modulation in 1.3-μm semiconductor lasers subject to strong injection locking," IEEE Photon. Technol. Lett. **16**, 972–974 (2004).
32. T. B. Simpson, "Mapping the nonlinear dynamics of a distributed feedback semiconductor laser subject to external optical injection," Opt. Commun. **215**, 135–151 (2003).
33. A. Gavrielides, V. Kovanis, and T. Erneux, "Analytical stability boundaries for a semiconductor laser subject to optical injection," Opt. Commun. **136**, 253–256 (1997).
34. T. B. Simpson and J. M. Liu, "Phase and amplitude characteristics of nearly degenerate four-wave mixing in Fabry-Perot semiconductor lasers," J. Appl. Phys. **73**, 2587–2589 (1993).
35. A. Murakami, K. Kawashima, and K. Atsuki, "Cavity resonance shift and bandwidth enhancement in semiconductor lasers with strong light injection," IEEE J. Quantum Electron. **39**, 1196–1204 (2003).
36. S. K. Hwang and D. H. Liang, "Effects of linewidth enhancement factor on period-one oscillations of optically injected semiconductor lasers," Appl. Phys. Lett. **89**, 061120 (2006).
37. W. A. van der Graaf, A. M. Levine, and D. Lenstra, "Diode lasers locked to noisy injection," IEEE J. Quantum Electron. **33**, 434–442 (1997).
38. S. K. Hwang and J. M. Liu, "Dynamical characteristics of an optically injected semiconductor laser," Opt. Commun. **183**, 195–205 (2000).
39. S. Wieczorek, B. Krauskopf, and D. Lenstra, "A unifying view of bifurcations in a semiconductor laser subject to optical injection," Opt. Commun. **172**, 279–295 (1999).
40. T. Erneux, V. Kovanis, A. Gavrielides, and P. M. Alsing, "Mechanism for period-doubling bifurcation in a semiconductor laser subject to optical injection," Phys. Rev. A. **53**, 4372–4380 (1996).
41. H. S. Ryu, Y. K. Seo, and W. Y. Choi, "Optical single sideband modulation using an injection-locked semiconductor laser as an optical filter," Intl. Topical Meeting on Microwave Photonics, 223–226 (2003).
42. S. C. Chan and J. M. Liu, "Microwave frequency division and multiplication using an optically injected semiconductor laser," IEEE J. Quantum Electron. **41**, 1142–1147 (2005).

1. Introduction

Microwave photonics has gained much attention over the past decade [1, 2]. An important driving force behind the technology is the need for transmitting microwave subcarriers through optical fibers. Such radio-over-fiber (RoF) systems are capable of distributing microwave signals over long distances [3–5]. However, most RoF systems are subject to the chromatic dispersion-induced microwave power penalty [6,7]. Because the dispersion introduces a phase difference between the sidebands from the optical carrier, the generated beat signals between the sidebands and the carrier may add up destructively depending on their phase relationship. This results in a reduction of the generated microwave power.

Power penalty can be avoided by using the single sideband (SSB) modulation scheme. A number of SSB optical microwave sources have been reported, including heterodyning two lasers [8–10], SSB external modulators [5, 7, 11], dual-mode or multisection semiconductor lasers [6, 12–15], and filtering directly modulated semiconductor lasers [16]. Each approach has its own advantages and challenges. The heterodyne method is usually widely tunable, but it requires fast and complicated electronics for optical phase locking. The external modulation method does not require optical phase locking, but the modulators are usually quite lossy and they require high driving voltages. The dual-mode laser method can be realized by using various compact multisection designs, but the generated microwave signals have limited tunability because of the fixed cavity lengths. The filtering method is straightforward, but the microwave frequency and the modulation depth are limited by the modulation bandwidths of the semiconductor lasers.

In this paper, we investigate an optically injected semiconductor laser [17, 18]. The laser is operated under the nonlinear dynamical period-one oscillation state. It generates

#83240 - $15.00 USD Received 21 May 2007; revised 21 Oct 2007; accepted 22 Oct 2007; published 26 Oct 2007

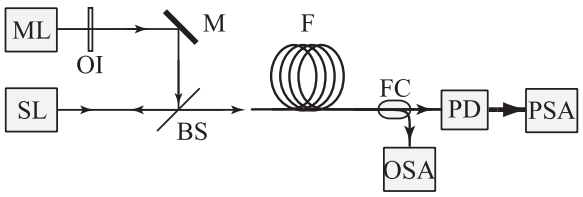

Fig. 1. Schematic of the simulated setup. ML: master laser; SL: slave laser; OI: optical isolator; M: mirror; BS: beam splitter; F: fiber; FC: fiber coupler; PD: photodiode; PSA: power spectrum analyzer; and OSA: optical spectrum analyzer.

microwave signal on an optical wave. Previous work has shown that the microwave signal can be widely tuned [19], optically controlled [17, 20], and easily locked [21–27]. When properly controlled, the period-one states possess SSB spectra as well. These properties enable the optical injection system to be an ideal RoF source. However, to the best of our knowledge, there is no comprehensive investigation conducted on the SSB characteristics of the system and the associated immunity to the power penalty. We address these issues in this paper. Comprehensive numerical simulations of the system are conducted over a wide range of injection strengths and frequency detunings. Double sideband (DSB) and SSB period-one states are found under different injection conditions. The results serve as a guideline for optimizing the systems for practical RoF applications.

By using the period-one oscillation state, the system generates a microwave frequency that is tunable up to 6 times the relaxation oscillation frequency. A microwave frequency higher than 60 GHz can be obtained. The wide tunability is made possible by the laser nonlinear dynamics. If the system is applied for data communication, the data bandwidth is typically much smaller than the microwave subcarrier frequency. Therefore, the power penalty calculation presented in this paper is valid even when data is included. Though the details of data modulation is not considered here, various methods of modulating the period-one oscillation has been documented previously [17, 21, 25]. On one hand, frequency-modulated period-one oscillation has been demonstrated [17]. The method utilizes the optical controllability of the nonlinear state. Amplitude-to-frequency modulation conversion is achieved together with upconversion. On the other hand, injection-locked period-one state has also been demonstrated using a double-lock technique [21, 25]. The method applies an external microwave data signal to lock the period-one state. In some RoF applications, the baseband data and the microwave subcarrier are simultaneously transmitted over fiber [26]. Microwave upconversion is performed remotely at the base stations. For the above reasons, this paper is intended to focus only on the generation and transmission of the unmodulated period-one state.

Following this introduction, the simulation model is presented in Section 2. Detailed numerical results are reported in Section 3. They are followed by discussions and conclusion in Sections 4 and 5, respectively.

2. Simulation model

The schematic of the setup considered is shown in Fig. 1. A master laser (ML) is optically injected into a single-mode slave laser (SL). The output of the slave laser is sent through an optical fiber (F). The optical and the power spectra are monitored at the optical spectrum analyzer (OSA) and the power spectrum analyzer (PSA), respectively.

The slave laser can be described by the following rate equations of a single-mode

#83240 - $15.00 USD Received 21 May 2007; revised 21 Oct 2007; accepted 22 Oct 2007; published 26 Oct 2007

semiconductor laser under optical injection [28]:

$$\frac{\mathrm{d}A}{\mathrm{d}t} = \Big[-\frac{\gamma_\mathrm{c}}{2}+\mathrm{i}(\omega_0-\omega_\mathrm{c})\Big]A+\frac{\Gamma}{2}(1-\mathrm{i}b)gA+\eta A_\mathrm{i}\mathrm{e}^{-\mathrm{i}\Omega_\mathrm{i}t} \quad (1)$$

$$\frac{\mathrm{d}N}{\mathrm{d}t} = \frac{J}{ed}-\gamma_\mathrm{s}N-gS \quad (2)$$

where A is the complex intracavity field amplitude with respect to the free-running angular frequency ω_0 of the slave laser, γ_c is the cavity decay rate, ω_c is the cold cavity angular frequency, Γ is the confinement factor of the optical mode inside the gain medium, b is the linewidth enhancement factor, g is the optical gain, η is the injection coupling rate, A_i is the injection field amplitude, $f_\mathrm{i}=\Omega_\mathrm{i}/2\pi$ is the detuning frequency of the master laser with respect to $\omega_0/2\pi$, N is the charge carrier density, J is the injection current density, e is the electronic charge, d is the active layer thickness, γ_s is the spontaneous carrier relaxation rate, and S is the active region photon density. The photon density is related to the field by [29]:

$$S=\frac{2\epsilon_0 n^2}{\hbar\omega_0}|A|^2 \quad (3)$$

where ϵ_0 is the free-space permittivity, n is the refractive index, and $\hbar$ is the reduced Planck's constant. The gain is a function of N and S. It is given by [30]:

$$g=\frac{\gamma_\mathrm{c}}{\Gamma}+\gamma_\mathrm{n}\frac{N-N_0}{S_0}-\gamma_\mathrm{p}\frac{S-S_0}{\Gamma S_0} \quad (4)$$

where γ_n is the differential carrier relaxation rate, γ_p is the nonlinear carrier relaxation rate, and N_0 and S_0 are respectively the steady-state values of N and S when the slave laser is free-running. Equations (1) and (2) can be normalized using $a_\mathrm{r}+\mathrm{i}a_\mathrm{i}=A/|A_0|$ and $1+\tilde{n}=N/N_0$, where A_0 is the free-running A. The equations become:

$$\frac{\mathrm{d}a_\mathrm{r}}{\mathrm{d}t} = \frac{1}{2}\Big[\frac{\gamma_\mathrm{c}\gamma_\mathrm{n}}{\gamma_\mathrm{s}\tilde{J}}\tilde{n}-\gamma_\mathrm{p}(a_\mathrm{r}^2+a_\mathrm{i}^2-1)\Big](a_\mathrm{r}+ba_\mathrm{i})+\xi_\mathrm{i}\gamma_\mathrm{c}\cos\Omega_\mathrm{i}t \quad (5)$$

$$\frac{\mathrm{d}a_\mathrm{i}}{\mathrm{d}t} = \frac{1}{2}\Big[\frac{\gamma_\mathrm{c}\gamma_\mathrm{n}}{\gamma_\mathrm{s}\tilde{J}}\tilde{n}-\gamma_\mathrm{p}(a_\mathrm{r}^2+a_\mathrm{i}^2-1)\Big](-ba_\mathrm{r}+a_\mathrm{i})-\xi_\mathrm{i}\gamma_\mathrm{c}\sin\Omega_\mathrm{i}t \quad (6)$$

$$\frac{\mathrm{d}\tilde{n}}{\mathrm{d}t} = -\Big[\gamma_\mathrm{s}+\gamma_\mathrm{n}(a_\mathrm{r}^2+a_\mathrm{i}^2)\Big]\tilde{n}-\gamma_\mathrm{s}\tilde{J}(a_\mathrm{r}^2+a_\mathrm{i}^2-1) + \frac{\gamma_\mathrm{s}\gamma_\mathrm{p}}{\gamma_\mathrm{c}}\tilde{J}(a_\mathrm{r}^2+a_\mathrm{i}^2)(a_\mathrm{r}^2+a_\mathrm{i}^2-1) \quad (7)$$

where $\tilde{J}=(J/ed-\gamma_\mathrm{s}N_0)/\gamma_\mathrm{s}N_0$ is the normalized bias above the threshold current and $\xi_\mathrm{i}=\eta|A_\mathrm{i}|/\gamma_\mathrm{c}|A_0|$ is the dimensionless injection strength [28]. The values of the dynamic parameters are extracted from a typical semiconductor laser. Their values are as follows [31]: $\gamma_\mathrm{c}=5.36\times10^{11}$ s^{-1}, $\gamma_\mathrm{s}=5.96\times10^{9}$ s^{-1}, $\gamma_\mathrm{n}=7.53\times10^{9}$ s^{-1}, $\gamma_\mathrm{p}=1.91\times10^{10}$ s^{-1}, $b=3.2$, and $\tilde{J}=1.222$. The relaxation resonance frequency is given by $f_\mathrm{r}=(2\pi)^{-1}(\gamma_\mathrm{c}\gamma_\mathrm{n}+\gamma_\mathrm{s}\gamma_\mathrm{p})^{1/2}\approx10.25$ GHz [30]. Numerically, we conduct a second-order Runge-Kutta integration for a duration longer than 1 μs. The injection strength ξ_i is varied between 0 and 0.4, while the frequency detuning f_i is varied between -10 and 60 GHz. We consider mainly positive f_i because the period-one state is usually seen for positive detunings. Negative f_i leads to stable locking and mode hopping dynamics [32]. The optical and the power spectra are obtained from the Fourier transforms of $a_\mathrm{r}+\mathrm{i}a_\mathrm{i}$ and $|a_\mathrm{r}+\mathrm{i}a_\mathrm{i}|^2$, respectively. The effect of the fiber dispersion will be treated in Section 3.4.

#83240 - $15.00 USD Received 21 May 2007; revised 21 Oct 2007; accepted 22 Oct 2007; published 26 Oct 2007

3. Numerical results

The numerical results are presented as follows. The evolution of the period-one oscillation state is first presented. It is followed by the mapping of the generated microwave frequency and the corresponding microwave power. The effect of the fiber chromatic dispersion on the power penalty is considered afterwards.

3.1. State evolution

The injection frequency detuning is kept constant at $f_{\mathrm{i}} = 20$ GHz, while the injection strength ξ_{i} is varied. The evolution of the optical spectra that are centered at the free-running slave laser frequency is shown in Fig. 2. When $\xi_{\mathrm{i}} = 0.35$, shown in Fig. 2(a), the injection is strong enough to pull the slave laser to the injected frequency. The laser is stably locked at f_{i} [29]. When ξ_{i} is decreased to 0.29, shown in Fig. 2(b), the laser undergoes a Hopf bifurcation so that it develops an oscillation at a microwave frequency f_0. It is said to be in the period-one oscillation state [28, 33]. The spectrum consists of components separated from f_{i} by multiples of f_0. The main components are at $f_{\mathrm{c}} = f_{\mathrm{i}} - f_0$ and f_{i}. The next strongest component is at $f_{\mathrm{c}} - f_0$, but it is over 20 dB weaker than the two main components. Therefore, the signal is approximately SSB, which is desirable for RoF transmission. However, when ξ_{i} is reduced to 0.06, shown in Fig. 2(c), the period-one spectrum becomes nearly DSB. The carrier frequency at $f_{\mathrm{c}} = f_{\mathrm{i}} - f_0$ is surrounded by two equally strong sidebands. Also, the frequency separation f_0 is reduced. When ξ_{i} is further decreased to 0.01, shown in Fig. 2(d), the spectrum continues to be roughly double-sided. The microwave frequency f_0 is further decreased such that the carrier is now at $f_{\mathrm{c}} \approx 0$, which corresponds to the free-running frequency of the slave laser. The period-one state has gradually become a four-wave mixing state between the free-running slave laser and the optical injection [34], although a clear boundary between the two states cannot be determined here. Summarizing the state evolution under a decreasing ξ_{i}, the slave laser experiences stable locking, SSB period-one oscillation, DSB period-one oscillation, and, eventually, four-wave mixing. The microwave frequency f_0 also varies; its characteristics are elaborated below.

3.2. Fundamental microwave frequency

The beating of the optical components seen in Fig. 2 at the photodiode generates a microwave signal with the fundamental frequency of f_0. The dependence of f_0 as a function of ξ_{i} is shown in Fig. 3 for different values of f_{i}. When ξ_{i} is very small, the slave laser emits at its undisturbed free-running optical frequency. The injected light beats with the slave laser and thus generates $f_0 \approx f_{\mathrm{i}}$ at $\xi_{\mathrm{i}} \approx 0$ for all the curves. When ξ_{i} is gradually increased for the cases of $f_{\mathrm{i}} = 40$, 30, and 20 GHz, Fig. 3 shows that f_0 also increases accordingly. It can be qualitatively understood as a result of the red-shifting of the cavity resonance. When ξ_{i} increases, the optical gain deficit increases [29, 35]. Because of the antiguidance effect, the refractive index increases and thus the cavity resonance shifts red. The red-shifting causes the period-one oscillation frequency $f_{\mathrm{i}} - f_0$ to decrease. Hence, f_0 generally increases with ξ_{i} for a fixed f_{i}, which is observed in most of the related studies [19, 23, 28, 36]. However, exceptions to the general trend are found when the cavity red-shifting effect is opposed by another effect, the injection pulling effect. The pulling effect is explained by the Adler's equation that governs the phase dynamics of the laser [37]. As a weak injection progressively locks the optical phase of the slave laser, the injected field pulls the frequency of the intracavity field oscillation away from the cavity resonance towards the injected frequency. Hence, the pulling effect tends to reduce the frequency separation f_0.

#83240 - $15.00 USD Received 21 May 2007; revised 21 Oct 2007; accepted 22 Oct 2007; published 26 Oct 2007

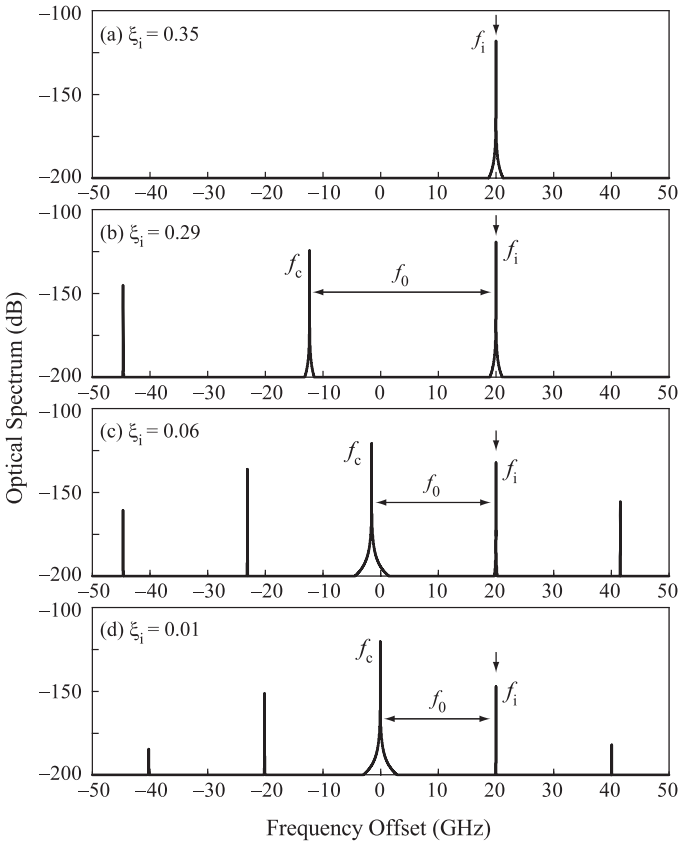

Fig. 2. Optical spectrum with the frequency offset to the free-running slave laser frequency. The injection frequency detuning is kept constant at $f_i = 20$ GHz as indicated by the arrows. The injection strength ξ_i is varied to obtain different states: (a) stable locking ($\xi_i = 0.35$); (b) SSB period-one ($\xi_i = 0.29$); (c) DSB period-one ($\xi_i = 0.06$); and (d) four-wave mixing ($\xi_i = 0.01$).

The dependence of f_0 on ξ_i is determined by whether the red-shifting effect or the injection pulling effect dominates. The competition between these two effects is illustrated by the curve of f_i =10 GHz in Fig. 3. For $\xi_i < 0.02$, f_0 decreases with ξ_i as a result of the progressive injection pulling en route to locking. For $\xi_i > 0.04$, f_0 obeys the general trend of increasing with ξ_i as the cavity red-shifting dominates. For $0.02 < \xi_i < 0.04$, f_0 changes abruptly because the laser enters the chaotic state. Since it is impossible to define a fundamental frequency for the broadband chaotic spectrum in a conventional sense, f_0 is numerically defined such that integrating the power spectrum from 0 to f_0 contains a certain fixed amount of power.

The dependence of f_0 on ξ_i and f_i is more clearly presented as a mapping in Fig. 4. A large region of period-one states is identified above the stable locking region across the Hopf bifurcation line. Period-two and chaotic regions are embedded within the period-one region when f_i is near the free-running relaxation resonance frequency, f_r [28,38,39]. The injection pulling effect dominates only at the confined regions indicated in Fig. 4, where f_i is small enough for the progressive pulling into locking to be significant. The slopes of the contour lines indicate that f_0 decreases with ξ_i. Other than these small

#83240 - $15.00 USD Received 21 May 2007; revised 21 Oct 2007; accepted 22 Oct 2007; published 26 Oct 2007

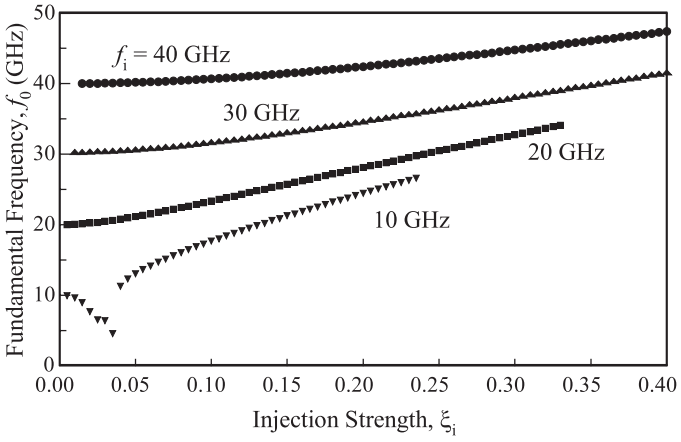

Fig. 3. Fundamental microwave frequency f_0.

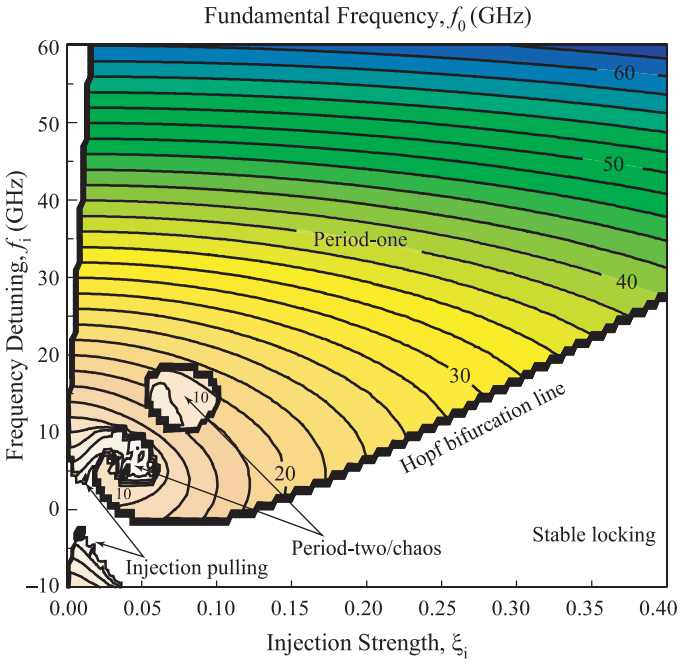

Fig. 4. Mapping of the fundamental frequency f_0.

#83240 - $15.00 USD Received 21 May 2007; revised 21 Oct 2007; accepted 22 Oct 2007; published 26 Oct 2007

and isolated regions in Fig. 4, the contour lines of constant f_0 reveal that f_0 increases with $\xi_{\rm i}$ in nearly the whole period-one region. The optical injection system is capable of generating widely tunable microwave signals of over 60 GHz, which is almost 6 times the free-running relaxation resonance frequency of the laser. Even higher frequencies can be obtained by increasing the detuning frequency until f_0 reaches the free-spectral range of the laser, where the single-mode model of the laser no longer applies. The free-spectral range is typically a few hundred gigahertz for an edge-emitting laser. Experimentally, period-one oscillation faster than 100 GHz has been observed in our system [17].

3.3. Microwave power

The optical frequency components in Fig. 2 separated by f_0 are converted into microwave signals at the photodiode. For RoF applications, it is important to understand how the generated microwave power varies with the injection parameters. The powers at the fundamental f_0 and the second harmonic $2f_0$ are denoted as P_{f_0} and P_{2f_0}, respectively. The fiber length is assumed to be zero here to illustrate the power variation before suffering from the chromatic dispersion power penalty. Figure 5 shows the variations of P_{f_0} and P_{2f_0} with respect to f_0. For each curve, the injection strength $\xi_{\rm i}$ is varied in order to tune the generated frequency f_0 while the injection detuning frequency $f_{\rm i}$ is kept constant. The circles, triangles, and squares correspond to $f_{\rm i}$ = 40, 30, and 20 GHz, respectively. The powers saturate soon after the period-one region is entered (Fig. 4). Also, the second harmonic is significantly weaker than the fundamental. The ratio P_{f_0}/P_{2f_0} is always larger than 20 dB. Therefore, the generated microwave is basically a sinusoid that is broadly tunable from 20 GHz to more than 40 GHz. Its power is also nearly constant over the whole frequency tuning range. The broad tunability with constant output power is an advantage of the period-one state over other photonic microwave sources. For completeness, the mapping of P_{f_0} is shown in Fig. 6. Since the absolute microwave power generated depends on the responsivity of the photodiode, all microwave power measurements in this paper are normalized to the peak value of P_{f_0}, which is shown in Fig. 6 as the 0-dB point at $\xi_{\rm i} = 0.095$ and $f_{\rm i}$ =5 GHz. Using a laser output of 1 mW, the microwave power at the 0-dB point is about -22 dBm when a typical 0.5 A/W detector is employed.

3.4. Dispersion-induced power penalty

We are now in a position to investigate the effect of fiber dispersion on the microwave transmission. Numerically, we first simulate the slave laser dynamics using Eqs. (1) and (2) to obtain the complex optical spectrum. The fiber dispersion is then modeled by introducing a frequency dependent phase into the spectrum. The phase is given by [30]:

$$\phi(\omega) = \frac{-\lambda^2 l D_\lambda}{4\pi c}(\omega - \omega_0)^2 \tag{8}$$

where ω is the optical angular frequency, λ is the wavelength, l is the fiber length, D_λ is the group-velocity dispersion, and c is the speed of light in free-space. We adopt typical values that $\lambda = 1.55$ μm and $D_\lambda = 17$ ps/km-nm, as in a Corning SMF-28 fiber. Fiber attenuation is neglected in this study. The modified optical spectrum is Fourier-transformed into time-domain optical field. The field is squared into intensity, which is transformed back to the frequency domain. The result is the power spectrum detected after the propagation through the fiber.

#83240 - $15.00 USD Received 21 May 2007; revised 21 Oct 2007; accepted 22 Oct 2007; published 26 Oct 2007

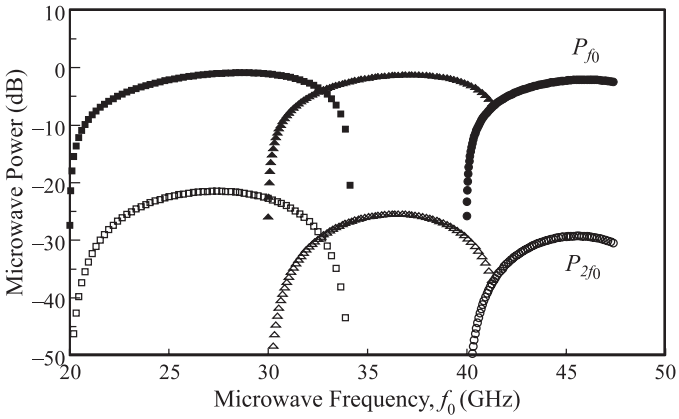

Fig. 5. Fundamental and second harmonic microwave power P_{f_0} (closed symbols) and P_{2f_0} (open symbols) as the generated microwave frequency f_0 is tuned. Tuning is achieved by varying ξ_i while keeping f_i constant at 40 GHz (circles), 30 GHz (triangles), and 20 GHz (squares), respectively.

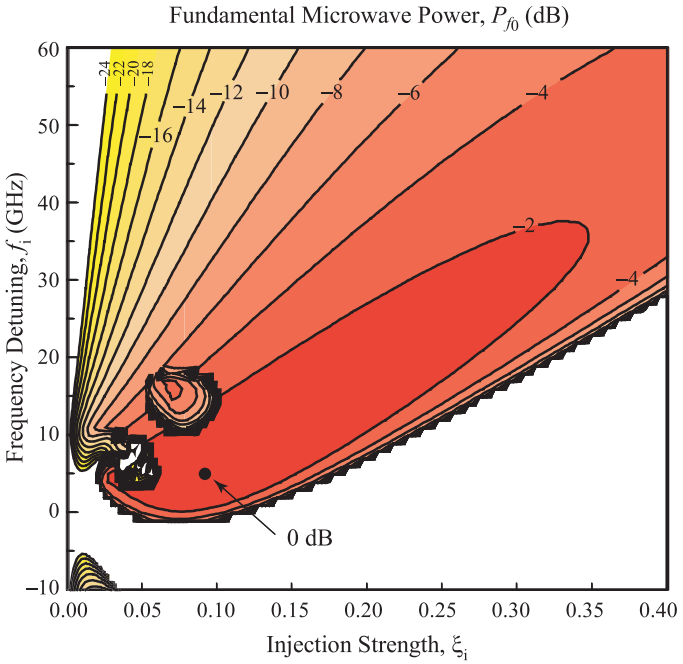

Fig. 6. Mapping of the fundamental microwave power P_{f_0} generated before transmitting over fiber. All microwave powers are normalized to the maximum power obtained at $(\xi_i, f_i) = (0.095, 5\ \text{GHz})$.

#83240 - $15.00 USD Received 21 May 2007; revised 21 Oct 2007; accepted 22 Oct 2007; published 26 Oct 2007

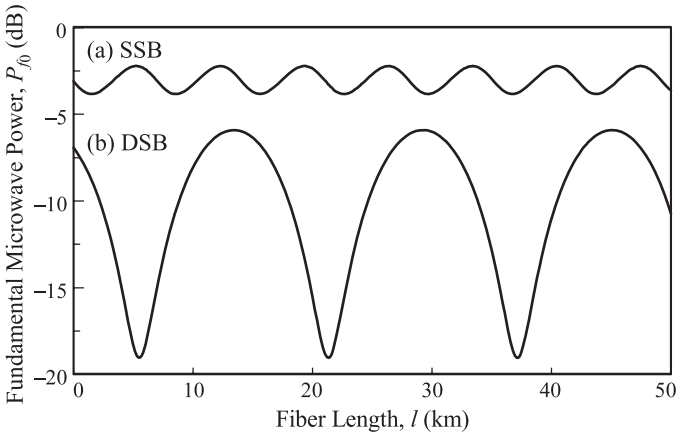

Fig. 7. Fundamental microwave power P_{f_0} generated after fiber propagation. The input period-one states are (a) SSB and (b) DSB, where ($\xi_{\rm i}$,$f_{\rm i}$)= (0.29, 20 GHz) and (0.06, 20 GHz), respectively.

3.4.1. Representative states

In order to illustrate the effect of dispersion on the period-one states, we consider the representative SSB and DSB period-one states presented in Fig. 2(b) and (c), respectively. The effect is shown in Fig. 7 as the generated P_{f_0} is plotted against the fiber length for both the SSB and the DSB period-one states. For the SSB case, it is apparent from the optical spectrum of Fig. 2(b) that the microwave power P_{f_0} is generated mainly from the beating of the optical frequency components at $f_{\rm i}$ and $f_{\rm i} - f_0$. When propagated through the fiber, the phase difference between the two optical components changes. However, the phase difference does not strongly affect the magnitude of the beat signal. Therefore, the power P_{f_0} varies only slightly as the fiber distance varies, which is shown in Fig. 7(a).

On the other hand, the DSB period-one state behaves differently. According to the optical spectrum in Fig. 2(c), f_0 is generated from the beating between $f_{\rm i}$ and $f_{\rm i} - f_0$ and that between $f_{\rm i} - f_0$ and $f_{\rm i} - 2f_0$. Because the optical components at $f_{\rm i}$ and $f_{\rm i} - 2f_0$ are of comparable magnitudes, both of their beat signals with the common $f_{\rm i} - f_0$ are important to the microwave generated. The microwave is a coherent sum of the beat signals; therefore, P_{f_0} depends critically on their phase difference. As a result, when extra phases are acquired during the fiber propagation, the value of P_{f_0} varies significantly. It is shown in Fig. 7(b) that P_{f_0} varies significantly over the fiber distance. A maximum power penalty of about 12 dB is found in this case. Hence, it is obvious that a desirable injection condition should drive the slave laser to an SSB period-one state so as to mitigate the fluctuation of P_{f_0} over distance. We thus turn our attention to the dependence of the optical spectrum on the injection parameters.

3.4.2. SSB characteristics

Referring to the optical spectra in Figs. 2(b) and (c), the main optical components of the period-one state are situated at the frequency offsets of $f_{\rm i} - 2f_0$, $f_{\rm i} - f_0$, $f_{\rm i}$, and $f_{\rm i} + f_0$. In order to quantify the study of the optical spectrum, the field components are denoted here as $A_{f_{\rm i}-2f_0}$, $A_{f_{\rm i}-f_0}$, $A_{f_{\rm i}}$, and $A_{f_{\rm i}+f_0}$, respectively. Figure 8 shows the magnitudes of these components as $\xi_{\rm i}$ varies while $f_{\rm i}$ is kept constant at 30 GHz. The

#83240 - $15.00 USD Received 21 May 2007; revised 21 Oct 2007; accepted 22 Oct 2007; published 26 Oct 2007

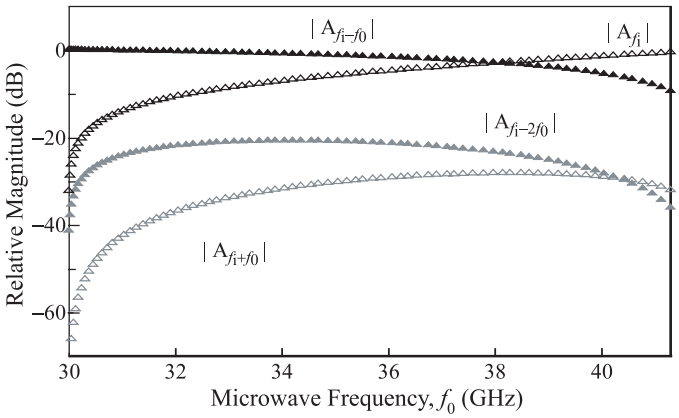

Fig. 8. Relative magnitudes of the optical frequency components as the generated microwave frequency f_0 is tuned. Tuning is achieved by varying ξ_i while keeping f_i constant at 30 GHz. The magnitudes are normalized to the free-running field amplitude $|A_0|$ of the slave laser.

curves of similar behaviors are also obtained at different values of f_i. A few general characteristics are observed:

- The magnitude of A_{f_i} increases with ξ_i because it is the direct regeneration of the optical injection.
- The magnitude of $A_{f_\mathrm{i}-f_0}$ gradually decreases as ξ_i increases because the gain is increasingly saturated and reduced by A_{f_i}. In the limit of $\xi_\mathrm{i} = 0$, the laser is free-running and $A_{f_\mathrm{i}-f_0} = A_0$. In fact, Fig. 8 is normalized to $|A_0|$.
- The strongest components are A_{f_i} and $A_{f_\mathrm{i}-f_0}$. Because they have opposite dependencies on ξ_i, their beat microwave signal P_{f_0} has a weaker dependence on ξ_i. (See Fig. 5.)
- The $A_{f_\mathrm{i}+f_0}$ component is usually the weakest among the four components shown. Thus, it can be neglected along with the other components not considered in Fig. 8, which are even weaker.

Therefore, the period-one state consists mainly of a central carrier $A_{f_\mathrm{i}-f_0}$, which is surrounded by the sidebands $A_{f_\mathrm{i}-2f_0}$ and A_{f_i}. A true SSB would consist of only the $A_{f_\mathrm{i}-f_0}$ and A_{f_i} components, whereas a balanced DSB has equal A_{f_i} and $A_{f_\mathrm{i}-2f_0}$ components. As shown in Fig. 8, $|A_{f_\mathrm{i}}|$ is much stronger than $|A_{f_\mathrm{i}-2f_0}|$ throughout almost the whole tuning range of f_0. Hence, the period-one state can be regarded as a broadly tunable SSB source.

The SSB characteristics can be quantified by the sideband rejection ratio that is defined here as $R = 20\log|A_{f_\mathrm{i}}/A_{f_\mathrm{i}-2f_0}|$. The dependence of R on ξ_i and f_i is calculated and presented as a mapping in Fig. 9. Although the period-one oscillation is DSB along the 0-dB contour line, there is a large region of increasingly SSB states as the operation point moves away from the region enclosed by the 0-dB line. At the proximity of the Hopf bifurcation line, states with A_{f_i} over 20 dB stronger than $A_{f_\mathrm{i}-2f_0}$ can be easily found, which can be practically regarded as an SSB signal [6]. It is desirable to operate the laser in this region such that the dispersion-induced power penalty is minimized.

#83240 - $15.00 USD Received 21 May 2007; revised 21 Oct 2007; accepted 22 Oct 2007; published 26 Oct 2007

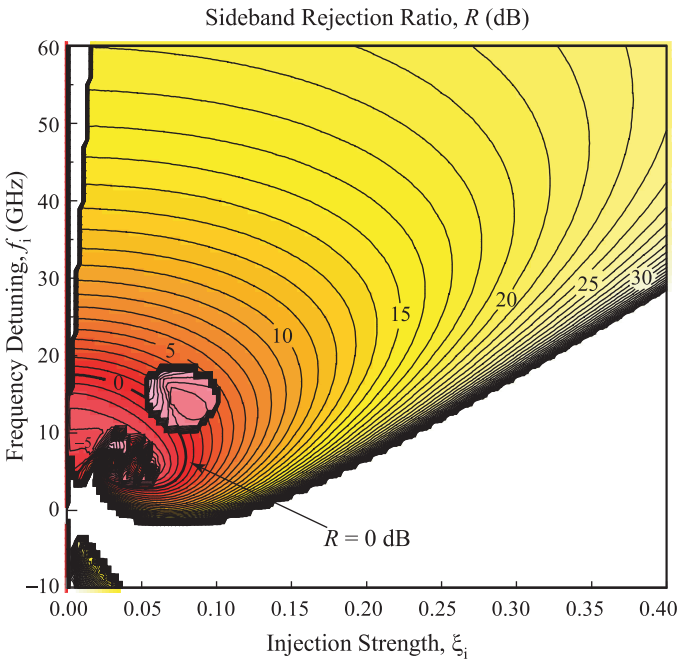

Fig. 9. Mapping of the sideband rejection ratio R.

3.4.3. Power penalty consideration

The main focus of this paper is to study the immunity of the SSB period-one states to the RoF power penalty. From the practical point of view, we are interested in knowing the minimum microwave power P_{f_0} that is guaranteed to a user at an arbitrary distance. The minimum power equals the power generated immediately after the laser (Fig. 6) minus the maximum power penalty. In other words, we are interested in finding the values of P_{f_0} at the minima of the curves similar to that of Fig. 7. The minimum power is shown as the mapping in Fig. 10. A peak of -3 dB is attained at $\xi_i = 0.25$ and $f_i = 20$ GHz. The high-power region around it is compared to the high-power region of Fig. 6. It is shifted towards the direction of increasing ξ_i because R, and the corresponding immunity to the power penalty, generally increases with ξ_i according to Fig. 9. Comparison to Fig. 4 shows that f_0 is still broadly tunable between 12 and 62 GHz when the injection condition is limited to within the -6-dB contour line of Fig. 10. It is also interesting to note that a remanent of the contour line of $R = 0$ dB in Fig. 9 is clearly visible in Fig. 10 because the corresponding DSB states are very much prone to the power penalty. Therefore, from these main features of the map, the laser is best operated under strong injection that is detuned slightly above the Hopf bifurcation line.

In short, the numerical results obtained from Eqs. (1) and (2) reveal the characteristics of the period-one state as the injection parameters are varied. These results suggest that the optical injection system is suitable for generating microwave for RoF transmission. It is because the period-one state can be used to generate nearly constant microwave power and nearly SSB spectrum over a wide frequency tuning range.

#83240 - $15.00 USD Received 21 May 2007; revised 21 Oct 2007; accepted 22 Oct 2007; published 26 Oct 2007

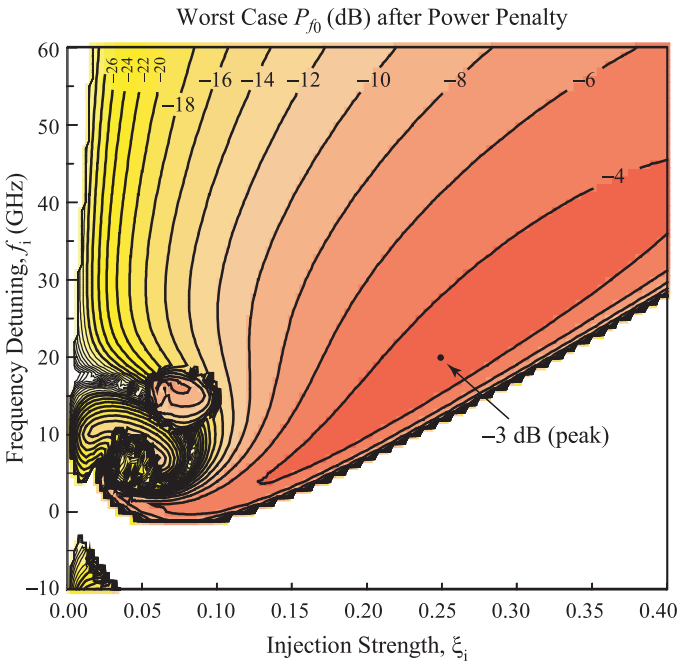

Fig. 10. Mapping of the worst case P_{f_0} when the dispersion-induced power penalty is considered.

4. Discussion

The RoF transmission is not subject to power penalty when the optical spectrum is SSB. The reason that most period-one states possess nearly SSB spectra can be qualitatively explained as follows. Due to optical injection, the time-averaged gain of the slave laser $\langle g \rangle$ is reduced from its free-running value γ_c/Γ. Through the coupling to the refractive index, the optical resonance of the cavity is shifted by

$$f_s = \frac{\Gamma}{4\pi} b \langle g - \frac{\gamma_c}{\Gamma} \rangle \tag{9}$$

which can be obtained by inspecting Eqs. (1) and (2). The frequency difference between the existing period-one component $A_{f_i - f_0}$ and the shifted cavity resonance is given by:

$$\Delta f = f_i - f_0 - f_s. \tag{10}$$

By applying Eq. (4) and the simulation results of (N, S) from Eqs. (1) and (2), Δf is obtained as shown in Fig. 11, which shows that $|\Delta f / f_0| \ll 1$. Thus $A_{f_i - f_0}$ receives the strongest enhancement from the frequency-shifted cavity among the other components of the optical spectrum. In addition, the other component, A_{f_i}, is strong because it is the direct regeneration of the injection. Therefore, there are two dominating optical components, namely, $A_{f_i - f_0}$ and A_{f_i}, which constitutes an SSB spectrum. This qualitatively explains the immunity to the power penalty for a large region of the period-one oscillations in the maps. Nevertheless, the analytical solution to the problem of the period-one optical spectrum is beyond our current scope [40].

Optically injected semiconductor lasers with the master laser being modulated by an external microwave source have been previously used for SSB applications [16, 41]. The

#83240 - $15.00 USD Received 21 May 2007; revised 21 Oct 2007; accepted 22 Oct 2007; published 26 Oct 2007

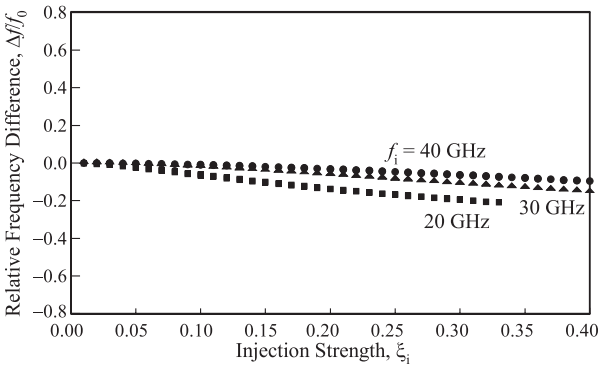

Fig. 11. Relative frequency difference $\Delta f/f_0$. Δf is the frequency difference between the period-one component $f_i - f_0$ and the shifted cavity resonance f_s.

direct modulation generates symmetric microwave sidebands. The slave laser then acts as an optical filter to select only the carrier frequency and one of the sidebands. By contrast, the system presented in this paper does not require any external microwave source. The nonlinear dynamics of the laser generates the microwave oscillation. Therefore, the method is not limited by the conventional direct modulation bandwidth [23]. In addition, because the generated frequency can be controlled optically, it can be applied for signal conversion such as AM-to-FM applications [17].

Lastly, the microwave linewidth of the period-one state can also be simulated by including the Langevin noise term into Eqs. (1) and (2) [28]. Although not considered in the preceeding treatment, the linewidth can be easily narrowed experimentally because all the optical components are related to each other inside the slave laser. Microwave linewidth narrowing using various simple techniques have been experimentally demonstrated [21–27]. The results show the reduction of microwave phase noise over a large range of operating conditions [23, 42]. This is an advantage over simple heterodyning two lasers that often requires fast and complicated optical phase-locking electronics [9].

5. Conclusion

In conclusion, the RoF performance of the period-one oscillation generated by an optically injected semiconductor laser is numerically investigated. The laser is shown to generate microwave frequency of up to 6 times its free-running relaxation resonance frequency. Over the wide tuning range of the generated frequency, the period-one state gives nearly constant microwave output power. Furthermore, the SSB characteristics of the optical spectrum and their implication in the immunity to the chromatic dispersion-induced microwave power penalty are also studied. Nearly SSB operation can be obtained over the broad tuning range. As a result, even with the worst case power penalty considered, the period-one state can be broadly tuned while keeping only a small variation in the output microwave power. The results suggest that the period-one state of the optically injected semiconductor laser is an attractive source for delivering microwave signals over fibers.

Acknowledgments

S.K. Hwang's work is supported by the National Science Council of Taiwan under Contract No. NSC96-2112-M-006-021.

#83240 - $15.00 USD Received 21 May 2007; revised 21 Oct 2007; accepted 22 Oct 2007; published 26 Oct 2007